Supplementary Information for:

Decoding frequency-modulated signals increases information entropy in bacterial second messenger networks

Rongrong Zhang [1,2†], Shengjie Wan [1,2†], Jiarui Xiong [3,1], Lei Ni [1,2], Ye Li [1,2], Yajia Huang [1,2], Bing Li [1,2], Mei Li [1,2], Shuai Yang [4,5*], Fan Jin [1,2*]

[1]CAS Key Laboratory of Quantitative Engineering Biology, Shenzhen Institute of Synthetic Biology, Shenzhen Institute of Advanced Technology, Chinese Academy of Sciences, Shenzhen, 518055, China.

[2]Shenzhen Synthetic Biology Infrastructure, Shenzhen Institute of Synthetic Biology, Shenzhen Institutes of Advanced Technology, Chinese Academy of Sciences, Shenzhen, 518055, China.

[3]Hefei National Research Center for Physical Sciences at the Microscale, Department of Polymer Science and Engineering, University of Science and Technology of China, Hefei, 230026, China.

[4]National Science Library (Chengdu), Chinese Academy of Sciences, Chengdu, 610299, China.

[5]Department of Information Resources Management, School of Economics and Management, University of Chinese Academy of Sciences, Beijing, 100049, China.

*Corresponding author(s). E-mail(s): Fan Jin, fan.jin@siat.ac.cn; Shuai Yang, yangs@clas.ac.cn;

†RongRong Zhang and Shengjie Wan contributed equally to this work.

Contents

Section 1: Supplementary Notes

Supplementary Note 1: Derivation of the Formula for the M1

In order to streamline the computation of the M1 segment, we posit that the deactivation of bPAC* is instantaneous, halting the synthesis of cAMP immediately upon the cessation of light. Denoting the concentration of cAMP as $x(t)$, with x_1 and x_2 representing the concentrations during light and dark phases, respectively, we can derive the following system of differential equations:

$$\begin{cases} \frac{\mathrm{d}x_1}{\mathrm{d}t} &= k - \gamma x_1, \\ \frac{\mathrm{d}x_2}{\mathrm{d}t} &= -\gamma x_2, \end{cases} \tag{1}$$

where k denotes the synthesis rate of cAMP influenced by bPAC* , note that this k includes the influence of [bPAC*], which leads $k = k_0$[bPAC*], and here [bPAC*] represents the concentration of light-activated bPAC, and γ signifies the hydrolysis rate of cAMP catalyzed by CpdA. The concentration fluctuations of cAMP constitute a periodic signal. It increases during light exposure and decreases during darkness. Therefore, the concentration at the start of each light period corresponds to a trough, while the concentration at the onset of darkness corresponds to a peak. Denoting the initial concentration at the onset of the peak and through value as x_{L} and x_{H} respectively .

After the system reaches equilibrium following n periods, taking this moment as the starting point $t = 0$, consider the signal output process for the $n + 1$ period: During the pulse signal duration TD, the cAMP concentration can be considered to rise from an initial value of x_{L}; in the remaining time $TD - T$ without a signal, it decays from an initial value of x_{H}. Therefore, we derive the following solutions for x_1 and x_2:

$$\begin{cases} x_1 = \left(x_{\mathrm{L}} - \dfrac{k}{\gamma}\right) e^{-\gamma t} + \dfrac{k}{\gamma} & 0 \le t \le TD \\ x_2 = x_{\mathrm{H}}\, e^{-\gamma(t-TD)} & TD \le t \le T \end{cases} \tag{2}$$

Hence, with regard to periodic input, the cAMP concentration at the conclusion of the light phase equals the concentration at the inception of the dark phase, designated as x_{H} (representing the peak value of the periodic oscillation). Correspondingly, the concentration at the conclusion of the dark phase aligns with the concentration at the onset of the light phase, denoted as x_{L} (representing the

trough value of the periodic oscillation). Subsequently, we derive:

$$\begin{cases} x_{\mathrm{H}} = \dfrac{k}{\gamma} \cdot \dfrac{1 - e^{-\gamma DT}}{1 - e^{-\gamma T}}, \\ x_{\mathrm{L}} = \dfrac{k}{\gamma} \cdot \dfrac{e^{\gamma DT} - 1}{e^{\gamma T} - 1}. \end{cases} \tag{3}$$

To validate our findings, we conducted dynamic simulations using MATLAB-SimBiology. The results are presented in Fig. 1d, where the horizontal axis represents the scaled period $\phi = \gamma T$ (with γ denoting the cAMP hydrolysis rate and T representing the actual period), while the vertical axis depicts the normalized amplitude of cAMP, relative to the maximum value under the current conditions, $[\mathrm{cAMP}]_{\max} = k/\gamma$.

Upon comparing the derived formulas with the simulation outcomes, we affirm the reliability of the established formulas thus far. Employing the aforementioned scaling approach and introducing $\tau = \gamma t$, akin to $\phi, s_1, s_2, s_{\mathrm{H}}, s_{\mathrm{L}}$ represent the scaled values of $x_1, x_2, x_{\mathrm{H}}, x_{\mathrm{L}}$ normalized by $[\mathrm{cAMP}]_{\max}$.

$$\begin{cases} s_{\mathrm{H}} = \frac{1-e^{-\phi D}}{1-e^{-\phi}} \\ s_{\mathrm{L}} = \frac{e^{\phi D}-1}{e^{\phi}-1} \end{cases} \tag{4}$$

Supplementary Note 2: Derivation of the Formula for the M2

As a secondary messenger, cAMP regulates protein transcription through two sequential Hill reactions. cAMP forms a complex with the regulatory protein Vfr, resulting in the formation of the Vfr-cAMP complex. Assuming an apparent dissociation constant of K_1 and a Hill coefficient of $n = 2$ for the binding reaction, with the protein Vfr being constitutively expressed. For clarity, denote the initial average concentrations of Vfr and Plac as $[\mathrm{Vfr}]_0$ and $[\mathrm{Plac}]_0$ respectively, and represent the cAMP concentration as [cAMP].

The binding of the Vfr-cAMP complex to the promoter Plac is assumed to have an apparent dissociation constant of K_2 and a Hill coefficient of $n = 1$ for the binding reaction. Assuming rapid equilibrium is reached in the reaction, the concentration of the activated-DNA at equilibrium is denoted as [Activated-Plac].

The following relationships can be delineated:

$$\begin{cases} [\text{Vfr-cAMP Complex}] = \dfrac{[\text{Vfr}]_0\ [\text{cAMP}]^2}{K_1^2 + [\text{cAMP}]^2} \\ [\text{Activated-Plac}] = \dfrac{[\text{Plac}]_0\ [\text{Vfr-cAMP Complex}]}{K_2 + [\text{Vfr-cAMP Complex}]} = \dfrac{[\text{Plac}]_0}{1 + \dfrac{K_2}{[\text{Vfr}]_0}\left[1 + \left(\dfrac{K_1}{[\text{cAMP}]}\right)^2\right]} \end{cases} \tag{5}$$

Both Hill binding reactions adhere to the same principle. A dynamic simulation was executed to validate the association between the initial concentration of cAMP and the activation state of the final product following two Hill reactions, illustrated in Fig. 2e. This figure vividly portrays that the equations aptly encapsulate the kinetic attributes of the reaction.

Supplementary Note 3: Derivation of the Formula for the M3

In accordance with the gene circuit designed in Fig. 1b, we will fuse GFP fluorescent protein as the output of the genetic circuit after activating the promoter Plac. Upon determining the concentration of Activated-Plac, the protein expression level can be viewed as the linear amplification of the promoter:

$$[\text{GFP}] = \frac{k_{\text{trans}}}{k_{\text{deg}}}[\text{Activated-Plac}] = \frac{k_1\ k_2}{k_{\text{deg1}}\ k_{\text{deg2}}} \frac{[\text{Plac}]_0}{1 + \dfrac{K_2}{[\text{Vfr}]_0}\left[1 + \left(\dfrac{K_1}{[\text{cAMP}]}\right)^2\right]} \tag{6}$$

We reduce the GFP concentration by $\frac{k_{\text{trans}}}{k_{\text{deg}}}[\text{Plac}]_0$. In order to simplify the expression, we introduce $\alpha = \frac{k}{\gamma K_1}$ and $\lambda = \frac{[\text{Vfr}]_0}{K_2}$. By substituting the reduced cAMP concentration $s(\tau)$, we derive:

$$\psi(\tau) = \frac{\lambda\alpha^2 s(\tau)^2}{1 + (\lambda+1)\alpha^2 s(\tau)^2} \tag{7}$$

This equation represents the integrand function. To determine the average value at the equilibrium state, we integrate it over one period from 0 to T. Due to the complexity of this integration, direct solutions are unattainable via mathematical or analytical methods. Thus, we resort to simplifying the formula to approximate a solution.

Upon examining the integrand $\psi(\tau)$, containing terms like $\lambda\alpha^2 s(\tau)^2$ and $(\lambda+1)\alpha^2 s(\tau)^2$ in both the numerator and denominator, if λ is sufficiently large, we can approximate $\lambda+1 \approx \lambda$. Experimental conditions validate this approximation. Consequently, we define $\theta \equiv \lambda\alpha^2 \approx (\lambda+1)\alpha^2$, which simplifies the integrand to: $\psi(\tau) = \dfrac{\theta s^2(\tau)}{1 + \theta s^2(\tau)}$.

Then, the ultimate objective is to compute the integral below, which quantifies the GFP production in one period at steady-state:

$$\bar{y} = f \int_0^{1/f} \frac{\theta s^2(\tau)}{1+\theta s^2(\tau)} \mathrm{d}\tau \tag{8}$$

Considering that one cycle can be segregated into two phases, illuminated and dark, the equation can be rephrased as:

$$\bar{y} = f \left(\int_0^{D/f} \frac{\theta s_1^2(\tau)}{1+\theta s_1^2(\tau)} \mathrm{d}\tau + \int_{D/f}^{1/f} \frac{\theta s_2^2(\tau)}{1+\theta s_2^2(\tau)} \mathrm{d}\tau \right) \tag{9}$$

By deriving $\frac{\mathrm{d}s_1}{\mathrm{d}\tau} = (1-s_\mathrm{L})e^{-\tau} = 1-s_1$ and $\frac{\mathrm{d}s_2}{\mathrm{d}\tau} = -s_\mathrm{H}e^{-\tau+D/f} = -s_2$, the equation is simplified to:

$$\begin{aligned} \bar{y} &= f \left(\int_{s_L}^{s_\mathrm{H}} \frac{\theta s_1^2}{(1+\theta s_1^2)(1-s_1)} \mathrm{d}s_1 + \int_{s_\mathrm{H}}^{s_\mathrm{L}} \frac{\theta s_2^2}{-s_2(1+\theta s_2^2)} \mathrm{d}s_2 \right) \\ &= f \int_{s_\mathrm{L}}^{s_\mathrm{H}} \frac{\theta s}{(1+\theta s^2)(1-s)} \mathrm{d}s \end{aligned} \tag{10}$$

After analysis, it is determined that: $s_\mathrm{H} = \dfrac{1-e^{-D/f}}{1-e^{-1/f}} = \dfrac{\sinh(\frac{D}{2f})}{\sinh(\frac{1}{2f})} e^{\frac{1-D}{2f}}$, $s_\mathrm{L} = \dfrac{e^{D/f}-1}{e^{1/f}-1} = \dfrac{\sinh(\frac{D}{2f})}{\sinh(\frac{1}{2f})} e^{-\frac{1-D}{2f}}$.

Using this, the integral can be solved with the aid of software like *Mathematica*, yielding:

$$\bar{y}(\theta, f, D) = f \left[\frac{\theta}{1+\theta} \ln \left(\frac{(1-s_\mathrm{L})\sqrt{1+\theta s_\mathrm{H}^2}}{(1-s_\mathrm{H})\sqrt{1+\theta s_\mathrm{L}^2}} \right) - \frac{\sqrt{\theta}}{1+\theta} \tan^{-1} \left(\frac{\sqrt{\theta}(s_\mathrm{H}-s_\mathrm{L})}{1+\theta s_\mathrm{H} s_\mathrm{L}} \right) \right] \tag{11}$$

Further, using the relation $D = f \ln\left(\frac{1-s_\mathrm{L}}{1-s_\mathrm{H}}\right)$, the equation simplifies to:

$$\bar{y}(\theta, f, D) = f \left[\frac{\theta}{1+\theta} \ln \left(\frac{\sqrt{1+\theta s_\mathrm{H}^2}}{\sqrt{1+\theta s_\mathrm{L}^2}} \right) - \frac{\sqrt{\theta}}{1+\theta} \tan^{-1} \left(\frac{\sqrt{\theta}(s_\mathrm{H}-s_\mathrm{L})}{1+\theta s_\mathrm{L} s_\mathrm{H}} \right) \right] + \frac{\theta D}{1+\theta} \tag{12}$$

If we refrain from simplifying using $\theta = \lambda\alpha^2 = (\lambda+1)\alpha^2$, the resulting equation would be:

$$\begin{aligned}\bar{y}(\alpha, f, D, \lambda) = f \Bigg[& \frac{\lambda\alpha^2}{1+(\lambda+1)\alpha^2} \ln\left(\frac{\sqrt{1+(\lambda+1)\alpha^2 s_{\mathrm{H}}^2}}{\sqrt{1+(\lambda+1)\alpha^2 s_{\mathrm{L}}^2}}\right) \\ & - \frac{\alpha\lambda/\sqrt{\lambda+1}}{1+(\lambda+1)\alpha^2} \tan^{-1}\left(\frac{\alpha\sqrt{\lambda+1}(s_{\mathrm{H}}-s_{\mathrm{L}})}{1+(\lambda+1)\alpha^2 s_{\mathrm{L}} s_{\mathrm{H}}}\right)\Bigg] \\ & + \frac{\lambda\alpha^2 D}{1+(\lambda+1)\alpha^2}\end{aligned} \tag{13}$$

Supplementary Note 4: Derivation of Threshold s^*

To simplify the given equation, we introduce a critical threshold, denoted as s^*, representing the cAMP concentration where the M2 filter achieves maximum sensitivity. By defining $\alpha = \frac{k}{\gamma K_1}$ and $\lambda = \frac{[\mathrm{Vfr}]_0}{K_2}$, we reduce the expression for the transcription factor-DNA binding to: $[\text{Activated-DNA}] = \dfrac{[\text{Plac}]_0\ [\text{Vfr-cAMP Complex}]}{K_2 + [\text{Vfr-cAMP Complex}]} = \dfrac{[\text{Plac}]_0}{1 + \frac{K_2}{[\mathrm{Vfr}]_0}\left[1 + \left(\frac{K_1}{[\mathrm{cAMP}]}\right)^2\right]}$.

By non-dimensionalizing [Activated-Plac] using $[\text{Plac}]_0$, we represent the dimensionless [Activated-Plac] as ψ and the dimensionless [cAMP] as s, leading to the simplified relationship: $\psi = \dfrac{1}{1 + \frac{1}{\lambda}\left(1 + \frac{1}{\alpha^2 s^2}\right)}$.

Due to the threshold filter being a second-order Hilbert function, we define the position where the curve changes most sensitively, namely where the second derivative is zero, as the threshold. To find the threshold, we solve for $\psi'' = 0$, resulting in: $s^* \equiv \sqrt{\dfrac{1}{3\alpha^2(1+\lambda)}}$.

Moreover, for $\psi'' = 0$, the condition $\alpha(1+\lambda) > \frac{1}{3}$ must be satisfied, a condition typically met in experimental setups.

This refined formulation represents a crucial step towards understanding the dynamics of the system, particularly in delineating the critical cAMP concentration where the M2 filter attains peak sensitivity.

Supplementary Note 5: Simplification of the analytical equation

Here we define y^* as the normalized protein expression level under continuous illumination, corresponding to a duty cycle of 1. Under continuous constant light intensity conditions (i.e., $D = 1, s_{\mathrm{H}} = s_{\mathrm{L}}$) , the steady-state average expression can be formulated as $y^* \equiv \bar{y}_{(\alpha,f,D=1,\lambda)} = \dfrac{\lambda\alpha^2}{1+(\lambda+1)\alpha^2}$. In the process of formula derivation,bPAC* undergoes instantaneous inactivation, and the issue of promoter leak expression is not considered. However, in specific genetic circuits, gene expression unavoidably includes leakage. To exclude these influences, we calculate Y, denoted as $Y = \dfrac{\bar{y}}{y^*}$. In experiments, Y is computed by subtracting the expression level of the unillumination group and then

dividing by the difference between the continuous illumination and unillumination group's expression levels.

$$Y = \frac{\bar{y}}{y^*} = D + f\left[\ln\left(\sqrt{\frac{1+(\frac{s_{\mathrm{H}}}{\sqrt{3}s^*})^2}{1+(\frac{s_{\mathrm{L}}}{\sqrt{3}s^*})^2}}\right) - \sqrt{3}s^*\left(\tan^{-1}\frac{\frac{s_{\mathrm{H}}}{\sqrt{3}s^*} - \frac{s_{\mathrm{L}}}{\sqrt{3}s^*}}{1+\frac{s_{\mathrm{H}}}{\sqrt{3}s^*}\frac{s_{\mathrm{L}}}{\sqrt{3}s^*}}\right)\right] \tag{14}$$

Introducing:

$$G = f\left[\frac{1}{2}\ln\left(\frac{1+(\frac{s_{\mathrm{H}}}{\sqrt{3}s^*})^2}{1+(\frac{s_{\mathrm{L}}}{\sqrt{3}s^*})^2}\right) - \sqrt{3}s^*\left(\tan^{-1}\frac{\frac{s_{\mathrm{H}}}{\sqrt{3}s^*} - \frac{s_{\mathrm{L}}}{\sqrt{3}s^*}}{1+\frac{s_{\mathrm{H}}}{\sqrt{3}s^*}\frac{s_{\mathrm{L}}}{\sqrt{3}s^*}}\right)\right] \tag{15}$$

, we propose that this signifies the impact of the frequency component of the input information on the ultimate output. Further simplification leads to $Y = \frac{\bar{y}}{y^*} = D+G$, where Y represents the relationship between the average output and the steady-state average expression.

Supplementary Note 6: Derivation of the relationship between s^* and D

Here, we will elucidate why under the condition $Y_{\mathrm{HF}} - Y_{\mathrm{LF}} = 0$, the relationship between D and s^* is established as $D = 3\ {s^*}^2$, as shown in Fig. 2b. It is crucial to emphasize that this is an idealized scenario and not practically attainable in experimental setups.

The difference between the high-frequency and low-frequency response is defined by $\bar{y}_{\mathrm{HF}} - \bar{y}_{\mathrm{LF}} = \lim_{f\to\infty}\bar{y} - \lim_{f\to 0}\bar{y}$.

When $\bar{y}_{HF}$ exceeds $\bar{y}_{LF}$, the genetic circuit is referred to as High-Pass FAC. Conversely, it is a Low-Pass FAC when $\bar{y}_{LF}$ exceeds $\bar{y}_{HF}$. To find the critical point, we calculate the scenario where the difference between $\bar{y}_{LF}$ and $\bar{y}_{HF}$ is zero.

Given $s_{\mathrm{H}} = \frac{1-e^{-D/f}}{1-e^{-1/f}}$ and $s_{\mathrm{L}} = \frac{e^{D/f}-1}{e^{1/f}-1}$, it follows that $\lim_{f\to\infty} s_{\mathrm{H}} = \lim_{f\to\infty} s_{\mathrm{L}} = D$, while $\lim_{f\to 0} s_{\mathrm{H}} = 1$, $\lim_{f\to 0} s_{\mathrm{L}} = 0$, as shown in Fig. 2d. Using these relations, we obtain: $\lim_{f\to\infty}\bar{y} = \frac{\lambda\alpha^2 D}{1+(\lambda+1)\alpha^2}$. To ensure $\bar{y}_{HF} = \bar{y}_{LF}$, it is required that $\lim_{f\to\infty}\bar{y} = \frac{\lambda\alpha^2 D}{1+(\lambda+1)\alpha^2}$, so as:

$$\lim_{f\to\infty}\left(\frac{1}{2}\frac{\lambda\alpha^2}{1+(\lambda+1)\alpha^2}\ln\left(\frac{1+(\lambda+1)\alpha^2 s_{\mathrm{H}}^2}{1+(\lambda+1)\alpha^2 s_{\mathrm{L}}^2}\right) - \frac{\alpha\lambda/\sqrt{\lambda+1}}{1+(\lambda+1)\alpha^2}\tan^{-1}\left(\frac{\alpha\sqrt{\lambda+1}(s_{\mathrm{H}}-s_{\mathrm{L}})}{1+(\lambda+1)\alpha^2 s_{\mathrm{L}}s_{\mathrm{H}}}\right)\right) = 0$$

. Furthermore, considering $\lim_{f\to\infty} s'_{\mathrm{H}}(f) = \frac{D(1-D)}{2}$ and $\lim_{f\to\infty} s'_{\mathrm{L}}(f) = -\frac{D(1-D)}{2}$, solving these equations leads to $D = 3(s^*)^2$. Therefore, when the relationship between D and s^* satisfies $D = 3(s^*)^2$, $\bar{y}_{HF} = \bar{y}_{LF}$.

Supplementary Note 7: Construction of the chassis strain for the FDCC.

In the construction of the FDCC, *Pseudomonas aeruginosa* PAO1 was meticulously selected as the foundational bacterium to ensure the precision of the cAMP synthesis and degradation pathways. This strain carries two cAMP synthesis genes (*cyaA*-*cyaB*) and one cAMP degradation gene (*cpdA*). For controlled signal input, the gene bPAC was specifically chosen for its involvement in blue light-induced cAMP synthesis. Initially, the synthesis genes *cyaA*-*cyaB* were removed from the PAO1 strain, and the gene fragment for persistent expression of the bPAC protein is inserted into the bacterial genome using the CTX system. To address biosafety concerns, the virulence factors ExoS and ExoT were methodically eliminated to enhance safety protocols. Ensuring data integrity and reliability required a strict emphasis on maintaining the bacteria in the logarithmic growth phase, achieved through continuous dilution and cultivation. However, challenges arose during continuous cultivation as PAO1 tended to form biofilms at the air-liquid interface, resulting in the presence of aggregates during sampling and potential inaccuracies in plate reader analyses. To tackle these issues, gene clusters *pslBCD* and *pelA* were systematically deleted to engineer a strain incapable of forming robust biofilms.

Consequently, the genotype of our chassis cells is: PAO1-Δ*pslBCD*Δ*pelA*Δ*exoS*Δ*exoT*Δ*cyaA* Δ*cyaB* , and this strain is designated as FAC01. Using the CTX transposon insertion method, we inserted a fragment containing the PA1/O4/O3 strong promoter and *bPAC* into the FAC01 genome, resulting in the creation of the FAC03 strain.

We utilized the CRISPR knockout method to achieve seamless deletion and insertion of segments in the PAO1 genome. The experimental protocol was optimized based on existing literature, using the deletion of the *cyaA* gene as a model. The detailed experimental procedure is outlined as follows:

1. Construction of Plasmid PCRISPR-*cyaA*:
   (a) Use the PAO1 genome as a template to PCR amplify around 500bp upstream and downstream homologous arms (*cyaA*-up and *cyaA*-dn segments), and obtain *cyaA*-up-dn segment through overlap amplification.
   (b) Amplify the N20-gRNA segment with primers containing the N20 segment.
   (c) Linearized plasmid vector segment PCRISPR.
   (d) Utilizing Gibson cloning technology, we successfully linked three segments to assemble the plasmid PCRISPR.
2. CRISPR-Cas9 Knockout Process:
   (a) Transform the plasmid PCASPA, which contains CAS9, into the PAO1 strain.
   (b) Select single clone colonies on an antibiotic plate with 100 µg/mL tetracycline.

(c) Incubate the colonies overnight in LB + tetracycline, dilute 1:50 in fresh LB, induce CAS9 expression with 0.02% arabinose, and continue culturing for 2 hours.

(d) Collect the bacterial culture, prepare electrocompetent cells, electroporate the plasmid PCRISPR-*cyaA*, and plate on a double-resistant plate with tetracycline and carbenicillin.

3. Gene Knockout Verification:

(a) PCR confirmation of the successful knockout of the target gene *cyaA* in the resulting colonies.

(b) Pick colonies and culture them overnight on LB agar plates without sodium chloride with 15% (wt) sucrose.

(c) Subculture colonies on LB plates containing tetracycline and carbenicillin to confirm complete plasmid loss.

(d) Sequence verification will confirm the PAO1-Δ*cyaA* strain.

Supplementary Note 8: Construction of FACs.

In our CRN and Theoretical model, the expression of *vfr* and *cpdA* genes is not affected by cAMP. However, in the wild-type PAO1 strain, their transcription is cAMP-regulated. Therefore, the initial step involves substituting their native promoters on the genome with persistent, cAMP-independent promoters in FAC03. This substitution will be achieved using CRISPR technology.

According to analytical formula predictions, the expression levels of *vfr*, *cpdA*, and *bPAC* directly impact the functionality of the FDCC (Supplementary Figure 3). Achieving an optimized frequency response in the FDCC necessitates precise regulation of these three genes' expression levels. This regulation entails fine-tuning their expression by manipulating promoters and Ribosome Binding Sites (RBS). Promoters such as J23106-J23115-J23110-J23100-J23102 and RBS variants like B0034-RBS046-RBS004-RBS017-RBS021 were employed in the experimental setup (doi: 10.1093/nsr/nwad031). Comprehensive details concerning the engineered strains are delineated in Supplementary Table 6.

The influence of these proteins on the performance of the FDCC is illustrated in Supplementary Figure 3. According to the theoretical curve, we needed to comprehensively adjust the expression levels of *vfr* and *cpdA*. Subsequently, after multiple optimizations, we obtained the bacterial strain FAC03C17V17 with a very pronounced High-Pass FAC.

The strain construction process adheres to the CRISPR gene insertion experimental protocol. For instance, in the replacement of the *vfr* upstream promoter with J23102-RBS017, a plasmid, J23102-RBS017-*vfr*-PCRISPR, is constructed. This plasmid contains the N20-gRNA, the insert fragment J23102-RBS017, and homologous segments. Utilizing the PAO1 genome as a template, integrate the

promoter and RBS sequences upstream of the *vfr* homologous through the PCR process. Subsequently, connect them to the downstream homologous arm of *vfr* via overlap PCR. Then, the specific N20-gRNA and UP-J23102-RBS017-DN fragments are inserted into the plasmid PCRISPR using the Gibson assembly technique. Following the CRISPR gene deletion approach, the plasmid is electroporated into FAC03 to yield strains with the replaced promoters, denoted as FAC03V17. Further replacement of the promoter preceding *cpdA* with J23100-RBS017 leads to a strain designated as FAC03C17V17-NP (without plasmid).

To measure the intracellular expression level of cAMP, we constructed a plasmid, Plac-*sfGFP*-T0T1-J23102-*CyOFP*-pJN105, and electroporated it into various chassis cells. The constitutively expressed CyOFP fluorescent protein serves as an internal standard for normalizing bacterial growth differences. The change in intracellular cAMP concentration is calculated by comparing the ratio of sfGFP to CyOFP.

Supplementary Note 9: Automated experimental workflow.

The bacterial culture, cultivated in FAB medium to the logarithmic phase, was aliquoted into a black 96-well plate, with 110 µL in each well. The OPCU device was then programmed via computer to input light control parameters such as intensity (I), period (T), duty cycle (D), and start time. Subsequently, a programmed automated experimental workflow was implemented to control the operation of the automation island. The automated workflow is shown in Supplementary Figure 4. Experimental consumables were positioned in PlateHotels on the automation island, initiating the automated experiment.

The detailed procedure of the automated experimental workflow is outlined as follows: The OPCU device, containing the bacterial culture, was initially transported by a robotic arm to the shaking incubator for a 20-minute incubation period, then moved to the Liquid Handlers for bacterial culture dilution. Subsequently, 50 µL of the culture was extracted and added to a Corning 3590 plate, which was then directed to the Microplate Reader for absorbance measurements at 600 nm and fluorescence intensity readings for sfGFP (470-520 nm), CyOFP (488-590 nm), and RFP (560-610 nm). Following measurements, the plate underwent cleaning at the Microplate Reader before being relocated to a designated area for subsequent dilution and measurement cycles. Adjusting the clamping direction of the robotic arms was necessary during the transfer process between the OPCU and the 96-well plate, requiring the use of a self-developed steering device. The bacterial culture in the OPCU was diluted 1:1 by adding 55 µL of fresh FAB medium, and the OPCU was then returned to the incubator for consistent incubation over 1 hour before the next dilution cycle. Pipette tips utilized for aspiration were cleaned sequentially with 75% ethanol and ultrapure water. Dilution procedures were conducted

hourly to maintain the bacteria's stable physiological state, ensuring precise characterization of the bacterial frequency response.

Supplementary Note 10: Quantitative characterization of the FDCC.

Based on the fluorescence intensity of fluorescent proteins measured by the Microplate Washer, we monitor the expression of corresponding promoters within bacteria. Due to the overlapping emission spectra of different fluorescent proteins, it is necessary to first calibrate the cross-talk coefficients between the fluorescence spectra. We diluted three purified fluorescent proteins, sfGFP, CyOFP, and mScarlet, and added them to the microplate. Using the plate reader, we measured the fluorescence intensity of each fluorescent protein in the channels of sfGFP (470-520 nm), CyOFP (488-590 nm), and RFP (560-610 nm) detection modes to calculate the cross-talk coefficients for each fluorescent protein in the other two channels. After correcting for cross-talk, we obtained the true fluorescence values for each fluorescent protein. In the 96-well plate of the OPCU, we set different light conditions, including continuous illumination with fixed intensity (a duty cycle of $D = 1$), unillumination ($D = 0$), and varying duty cycles between 0 and 1 during diverse illumination periods. Six periods were designated (100, 300, 500, 900, 1800, 2400 seconds).

By modifying the promoters and ribosome binding sites (RBS) in front of the genes *vfr* and *cpdA* in the genome, we have constructed a batch of bacterial strains with distinct frequency response characteristics. Strains containing plasmid Plac-*sfGFP*-T0T1-J23102-*CyOFP*-pJN105 were subjected to automated experiments, and optical density (OD_{600}) values along with fluorescence intensity values of sfGFP and CyOFP were obtained at different time points. Here, CyOFP served as an internal standard to eliminate errors arising from differences in bacterial quantity and state. Therefore, the output intensity of the FAC system could be calculated by dividing the fluorescence value of sfGFP by the value of CyOFP, which corresponds to the GR ratio in Supplementary Figure 5d. According to the calculation formula for Y in the analytical solution, we subtracted the GR ratio under a specific duty cycle from the corresponding unillumination condition, and then normalized by dividing the difference between the continuous illumination condition and the unillumination condition to obtain the Y value. Plotting the curve of Y against frequency variations and calculating the difference between Y_{HF} and Y_{LF} values can be used to evaluate the performance of the FAC system.

Supplementary Note 11: Theoretical fitting of experimental data.

For different bacterial strains and experimental conditions, the variables we need to fit include the initial concentration of bPAC (representing input light intensity, denoted as $[\text{bPAC}]_0$), as well as

the initial concentrations of CpdA ($[\text{CpdA}]_0$) and Vfr ($[\text{Vfr}]_0$), which are determined by the specific strain.

We perform the fitting by minimizing the least squares error between experimental data and MATLAB simulation data using the "lsqcurvefit" function from the MATLAB Optimization Toolbox. The fitting process minimizes the following objective function: $\min_x \|F(x, xdata) - ydata\|_2^2 = \min_x \sum_i (F(x, xdata_i) - ydata_i)^2$, where $xdata$ represents the experimental data, and $ydata$ represents the MATLAB simulation output. The function $F(x, xdata)$ is a matrix-valued or vector-valued function of the same size as $ydata$. The parameter x is a vector, where $x(1) = [\text{bPAC}]_0$, $x(2) = [\text{CpdA}]_0$, $x(3) = [\text{Vfr}]_0$. The function $F(x, xdata)$can be represented as: $F(x, xdata) = \begin{bmatrix} F(x, xdata)(1) \\ F(x, xdata)(2) \\ \vdots \\ F(x, xdata)(k) \end{bmatrix}$, and here $k = 3$.

Supplementary Note 12: Theoretical analysis of expanding bacterial state space through the FDCC.

Given that Vfr, functioning as a global regulatory factor, controls the expression of multiple target proteins within biological systems, it is imperative to examine how frequency-dependent regulation manifests its effects in this complex regulatory network. The following section provides a comprehensive discussion of these dynamics.

We denote the regulated proteins as $y_1, y_2, \cdots, y_n$, where the distinguishing feature among these proteins lies in their differential promoter binding affinities to the Vfr-$cAMP_2$ complex. These distinct binding characteristics are quantified by their respective λ parameters, designated as $\lambda_1, \lambda_2, \cdots, \lambda_n$. Without loss of generality, we adopt the convention that the subscript indices correspond to an ascending order of λ values, i.e., $\lambda_1 < \lambda_2 < \cdots < \lambda_n$. This hierarchical arrangement of λ parameters inherently results in a corresponding ordering of protein expression levels, establishing the relationship $y_1 < y_2 < \cdots < y_n$ under identical regulatory conditions. To facilitate comprehension and analytical tractability, we initiate our investigation by examining a simplified case where two proteins are under regulatory control.

Supplementary Note 12.1: Regulation via Dutycycle Modulation.

Our initial analysis focuses on the effects of pure amplitude control. The amplitude regulation is implemented through modulation of the duty cycle D, which induces differential expression levels of y_1 and y_2. To represent this regulatory mechanism geometrically, we introduce a parametric curve $L_2(D)$

in the two-dimensional protein expression space, with the subscript 2 indicating the dimensionality of the system. Specifically, $L_2(D) = (y_1(D), y_2(D))$.

In this two-dimensional coordinate system, the trajectory of the parametric curve $L_2(D)$ geometrically represents the manifold of attainable expression levels for the two regulated proteins, with each point on the curve corresponding to a specific regulatory state.

To convert the infinite number of points along the parametric curve into a finite set of discrete states, we employ a discretization parameter ϵ, as previously described in the main text. This parameter, which corresponds to the relative noise level in protein expression, effectively transforms the continuous expression space into a countable set of distinguishable regulatory states. For instance, setting $\epsilon = 0.1$ discretizes the two-dimensional expression space into a 10×10 lattice, with each grid cell corresponding to a unique and experimentally distinguishable expression state in the regulatory system. The total number of accessible regulatory states through amplitude control is quantified by counting the distinct cells traversed by the parametric curve $L_2(D)$. This phenomenon is clearly visualized in Fig. 4b, where the parametric curve exhibits the described characteristics.

Let l_2 denote the number of distinct grid cells traversed by the parametric curve in the two-dimensional expression space. The numerical results illustrated in the figure yield $l_2 = 19$, quantifying the number of distinguishable protein expression states accessible through duty cycle regulation. It is worth noting that in our numerical simulations, to guarantee that the parametric curve $L_2(D)$ reaches the point (1,1) in the expression space, we employ relatively large values for both the activation coefficient α and the binding affinity parameters λ.

Supplementary Note 12.2: Additional Control via Frequency Modulation.

A key characteristic of our experimental framework lies in the implementation of frequency-controlled genetic circuits. The introduction of frequency modulation as an additional control parameter, complementing duty cycle regulation, transforms the parametric curve into a surface in the two-dimensional expression space. This parameter-controlled surface, denoted as $S_2(D, f)$ where the subscript 2 indicates dimensionality, is defined by: $S_2(D, f) = (y_1(D, f), y_2(D, f))$.

Under the specified parameter conditions, the geometry of this parametric surface is depicted in the Figure 4b. We denote the number of distinct grid cells intersected by this surface as s_2, which numerical analysis reveals to be 38.

The graphical representation reveals that the parametric surface $S_2(D, f)$ is bounded by two prominent curves: a curvilinear boundary forming an arc, and a linear boundary along the diagonal. Given that the parametric surface arises from the incorporation of frequency modulation, we proceed to examine these two boundary curves through the lens of frequency-dependent regulation.

Drawing from our prior analysis of asymptotic behavior, when the modulation frequency f tends to zero, we have demonstrated that: $\lim_{f\to 0} \bar{y} = \frac{\theta}{1+\theta} D$. Given that $\theta \gg 1$, $\lim_{f\to 0} \bar{y} \approx D$. These findings reveal that in the zero-frequency limit, the expression levels y_1 and y_2 exhibit identical values, where their magnitudes are no longer influenced by the binding affinity parameter λ but are instead uniquely determined by the duty cycle D, such that $y_1 = y_2 = D$. This theoretical result explains the emergence of the diagonal boundary manifested in the parametric surface.

On the other hand, according to our previous asymptotic analysis, in the high-frequency limit, the following relationship holds: $\lim_{f\to\infty} \bar{y} = \frac{\theta}{\theta+1}(\frac{\theta D^2(1-D)}{1+\theta D^2} - \frac{D(1-D)}{1+\theta D^2} + D) \approx \frac{D^2+\theta D^2}{1+\theta D^2}$. Consequently, the second boundary curve is defined by the parametric trajectory $(\frac{D^2+\theta_1 D^2}{1+\theta_1 D^2}, \frac{D^2+\theta_2 D^2}{1+\theta_2 D^2})$. Our findings demonstrate that the spatial configuration of this parametric curve is governed by the parameters θ_1 and θ_2, which directly relate to the binding affinities λ_1 and λ_2. A significant observation is that increasing the differential between $\lambda_2$and $\lambda_1$causes the curve to asymptotically approach the piecewise linear path defined by the sequential vertices (0,0), (0,1), and (1,1).

Supplementary Note 12.3: *n*-Dimensional Analysis.

Having examined the regulatory outcomes of duty cycle and frequency modulation in a two-protein system, we now proceed to investigate the implications of expanding the number of regulated proteins. In the context of n regulated proteins, let $L_n(D)$ represent the parametric curve generated exclusively by duty cycle control, which maps to an n-dimensional expression space according to the following relationship: $L_n(D) = (y_1(D), y_2(D), \cdots, y_n(D))$.

The number of distinct grid cells traversed by this parametric curve in the n-dimensional expression space is denoted as l_n, quantifying the discrete states accessible through duty cycle modulation. Analogously, let $S_n(D, f)$ represent the n-dimensional parametric surface that emerges when frequency regulation is introduced, satisfying: $S_n(D, f) = (y_1(D, f), y_2(D, f), \cdots, y_n(D, f))$. Correspondingly, let $s_n$represent the count of distinct grid cells covered by the n-dimensional parametric surface $S_n(D, f)$.

While our primary aim is to investigate how l_n and s_n scale with increasing regulatory dimensionality (namely, the number of regulated proteins), a preliminary examination of other parameters' effects is warranted. In particular, the occupation number of n-dimensional grid cells by the parametric curve or surface is manifestly dependent on two other essential parameters: the binding affinity λ and the grid resolution ϵ. Alternatively, defining $r_n = \frac{s_n}{l_n}$ as the multiplicative factor by which frequency modulation expands the occupied grid space, we can represent it as: $r_n = F_1(\boldsymbol{\lambda})F_2(\epsilon)F_3(n)$.

The terms F_1, F_2, and F_3 appearing in this equation are functional components whose values are determined by three parameters: the binding affinity coefficient $\boldsymbol{\lambda}$, the discretization parameter ϵ, and the regulatory dimension n. The bold typeface in $\boldsymbol{\lambda}$ indicates a vector quantity $(\lambda_1, \lambda_2, ..., \lambda_3)$, where each component represents the binding affinity parameter of a distinct regulated protein.

Following the same reasoning as in our two-dimensional analysis, we observe that in the n-dimensional case, the relative magnitudes of binding affinities λ determine the geometric configuration of a boundary curve on the parametric surface. Specifically, as the difference among the λ values increases, this boundary curve exhibits a stronger tendency to converge toward a piecewise linear structure. The influence of the grid resolution parameter ϵ manifests through distinct power-law relationships: for the parametric curve, the number of occupied states scales inversely with ϵ ($l_n \propto \epsilon^{-1}$), whereas the parametric surface demonstrates a stronger inverse square dependence ($s_n \propto \epsilon^{-2}$).

As our central focus is on examining the dependence on regulatory dimension n, we conducted our numerical simulations with predetermined values of binding affinities λ and discretization parameter ϵ. In our numerical analysis implemented in MATLAB, we quantified the dimensional scaling of occupied states using a geometric sequence of binding affinities $(\lambda_1, \lambda_2, \cdots, \lambda_n) = (50, 50 \times 2^{2-1}, \cdots, 50 \times 2^{n-1})$ and a fixed discretization parameter $\epsilon = 0.1$. The resulting dependence of grid cell number on regulatory dimension n is illustrated in the Supplementary Figure. 6.

This result reveals a fundamental principle: when frequency-based regulation is introduced, the capacity for expanding the repertoire of gene expression states scales proportionally with the regulatory dimension, implying that larger gene network can achieve proportionally greater combinatorial diversity through frequency modulation. This property demonstrates a key biological implication of our frequency-to-amplitude conversion mechanism, establishing its fundamental role in enhancing the complexity and flexibility of gene regulatory networks.

Supplementary Note 13: Screening and characterization of cAMP-responsive promoters.

To screen for cAMP-responsive promoters, we selected 243 promoters regulated by the CRP-cAMP complex in *E. coli*. These promoters were then tested in the FAC03 to assess their responsiveness to regulation by the Vfr-cAMP$_2$ complex. Employing a 96-well optogenetic device (OPCU), we induced cAMP synthesis and utilized the native gene circuit for the Vfr transcription factor in *P. aeruginosa* wild type. Changes in bacterial fluorescence intensity were captured through microscopy. Promoter responsiveness was evaluated based on the ratio of fluorescence intensity between mScarlet and GFP.

By comparing the ratio after 10 hours of blue light exposure to the ratio at 0 hours, we conducted the preliminary screening to identify cAMP-responsive promoters (Supplementary Figure. 6).

Through initial screening, we identified 68 positive responsive promoters, which were then electroporated into the chassis cells FAC01V34C17B17. Subsequently, cAMP synthesis was induced using blue light, and automated experiments were conducted to further test dose-response curves under different light intensities, leading to the selection of 17 backup promoters. To further quantitatively characterize the frequency response curves of these promoters, a series of plasmids, Pro-*sfGFP*-J23102-*CyOFP*-pJN105, were constructed using the initially screened promoters. These plasmids were then electroporated into the chassis cells FAC03C17V17-NP, known for their excellent frequency response capabilities. The strains were tested under varying duty cycles and periods to evaluate the promoter response curves, and the sequences corresponding to the selected promoters can be found in Supplementary Table 8.

Supplementary Note 14: Designing experiments to verify the expansion of FAC in the bacterial gene expression space.

Based on the previously selected promoters with different frequency response characteristics, we linked them to various fluorescent proteins such as sfGFP, CyOFP, and mScarlet. These fragments were inserted into the genome of FAC03C17V17-NP or into plasmids. Initially, the nupGP-*sfGFP* fragment was inserted between the *PA3781* and *PA3782* genes in the genome, resulting in the strain named AutoRGB. Subsequently, we fused the nanAp promoter with mScarlet, constructing the plasmid nanAp-*mScarlet*-J23102-*CyOFP*-pJN105, which was then transformed into the FAC03V17V17-NP strain. This plasmid was further transformed into AutoRGB to create strain AutoRGB9. This strain allowed us to monitor the expression levels of nupGp on the genome and nanAp on the plasmid using sfGFP and mScarlet, respectively.

By calculating the ratios of sfGFP to CyOFP and the ratio of mScarlet to CyOFP, we obtained normalized outputs Y_{nupGp} and Y_{nanAp}. Then, we investigated how Y_{nupGp} varies with Y_{nanAp} under changing light intensities for a duty cycle of 1 and under different periods for fixed duty cycles ($D = 0.01, 0.03, 0.06, 0.1, 0.3, 0.5$), thereby depicting the two-dimensional space of bacterial states.Based on the analysis method in Note 12, the state intervals of duty cycle regulation and the state spaces of frequency regulation were depicted in the state space of Vfr regulation for the expression of two genes. Combined with the data fitting method in Note 11, the λ values of the two promoters nupGp and nanAp are 93 and 39 respectively. The results are presented in Fig. 4e. By introducing frequency

signals, the FAC system can effectively extend the spatial state, which is consistent with the theoretical results.

The J23102 promoter in front of *CyOFP* was replaced with the cAMP-regulated Plac promoter, leading to the creation of strain AutoRGB6. We quantitatively characterized the fluorescence intensity values of the three fluorescent proteins under different period duty cycles and corrected them with the corresponding values of OD_{600}. Subsequently, we normalized these values to obtain the expression protein Y values of the promoters, thereby depicting the three-dimensional space of bacterial states. Through automated experimental platforms, we conducted extensive input-response experiments under various conditions, including continuous illumination with varying light intensities and periodic illumination with different duty cycles.

The fluorescence data collected for sfGFP, CyOFP, and mScarlet were normalized and used to calculate the corresponding promoter outputs Y. It was observed that they distributed on a plane despite experimental noise, as shown in Fig. 4f, consistent with theoretical predictions. Subsequently, we fitted a polynomial surface to the experimental data using MATLAB. The boundaries of this parametric surface were defined by the maximum fluorescence values under continuous illumination and the minimum fluorescence values at different frequencies under periodic illumination. For visualization in Fig. 4f, we assigned a gradient of blue hues to the continuous illumination boundary curve and another gradient color scheme to the minimum values of different frequencies under periodic illumination. By simulating trajectories of frequency variations at constant duty cycles, the coloring scheme reflects both the relative position to the boundaries and the evolution patterns of different frequencies and duty cycles.

Section 2: Supplementary Figures

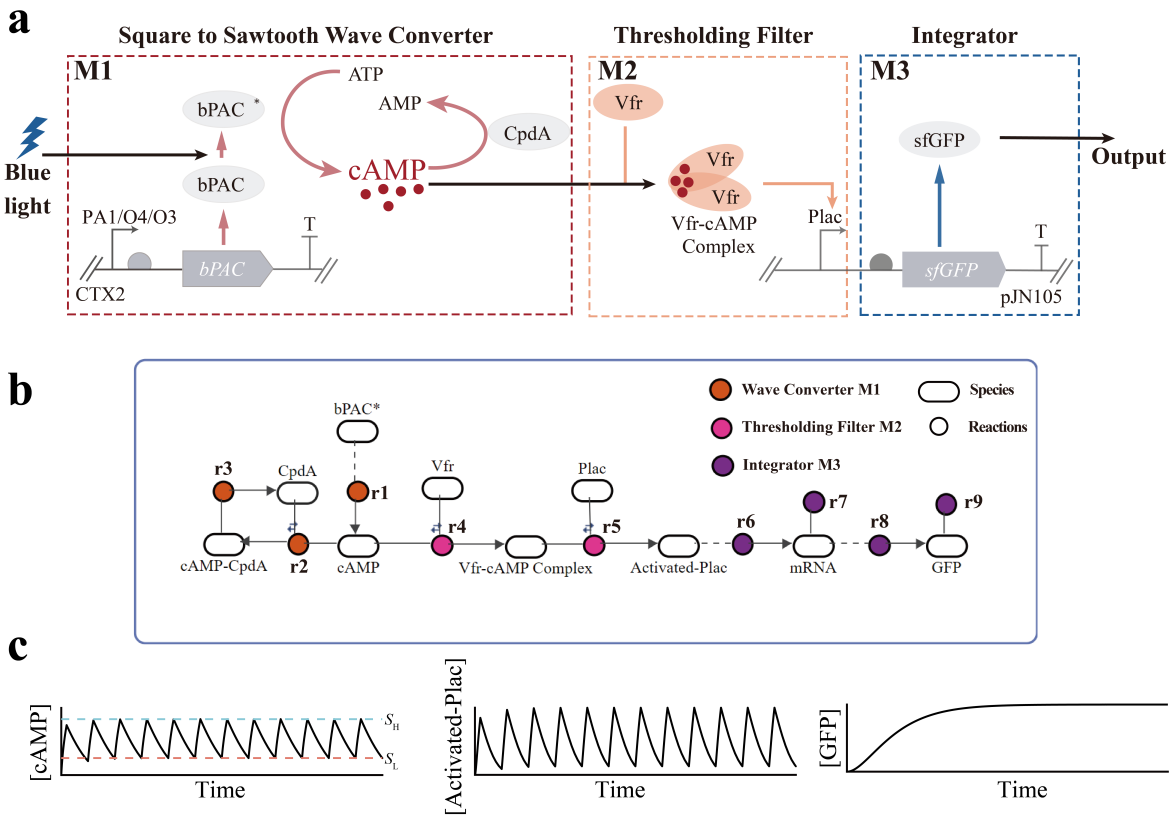

Supplementary Figure 1. The Chemical Reaction Network (CRN) model and simulation results corresponding to the FDCC. (a) Molecular implementation of the Frequency-Decoding cAMP Circuit (FDCC). Optogenetic circuit design incorporating light-activated bPAC and CpdA phosphodiesterase (M1), cAMP-dependent Vfr transcription factor binding (M2), and protein expression machinery (M3).bThe simplified CRN model utilized for simulation. The ellipses represent species in the FDCC, while the circles represent reactions. The organe, pink, and purple circles correspond to the kinetic reactions within modules Wave Converter (M1), Thresholding Filter (M2), and Integrator (M3), respectively. cAccording to the CRN model in the diagram (b), simulate the curves showing the concentrations of cAMP after passing through M1, activated DNA after passing through M2, and GFP after passing through M3, under a square wave periodic signal input.

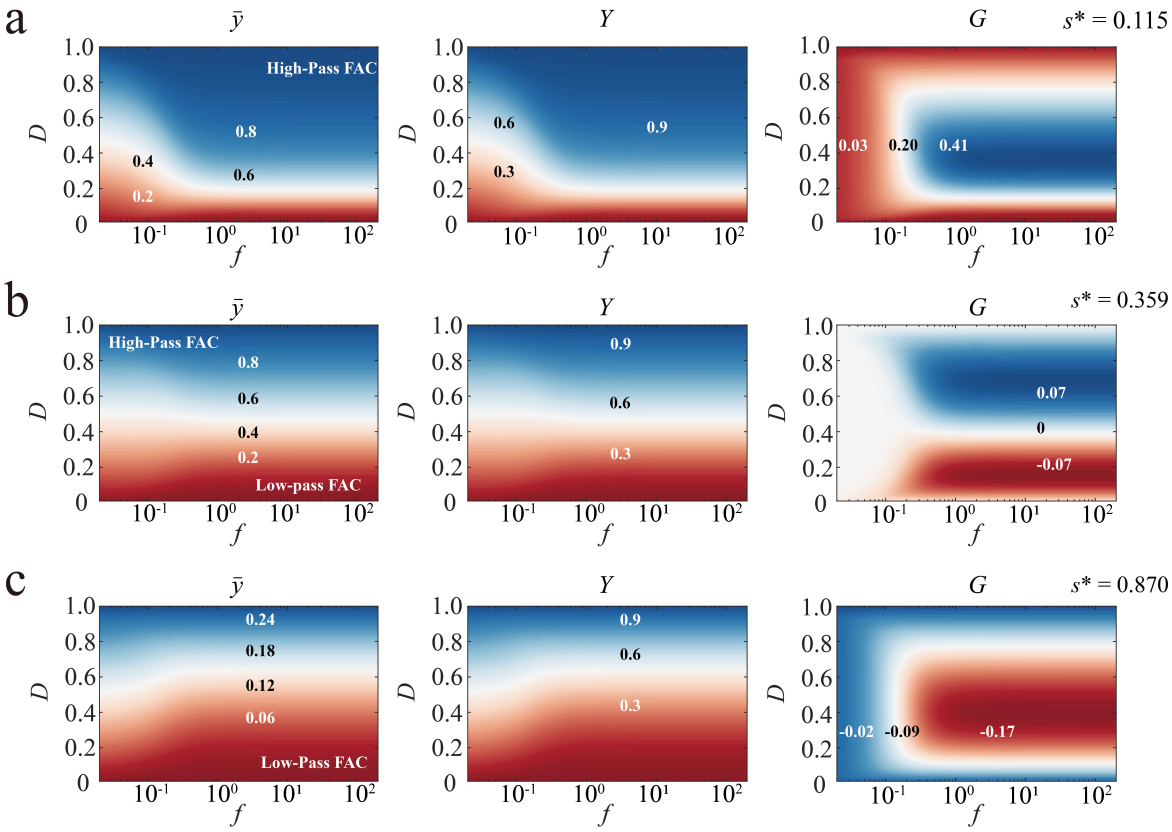

Supplementary Figure 2. Analysis of Factors Impacting FAC Performance. Explore the impact of frequency f and duty cycle D on the values of $\bar{y}$ calculated according to Formula 13, G computed by Formula 15, and Y obtained from Formula 14 in the main manuscript under varying threshold s^*. (a) At a threshold of 0.115, G is positive. Both $\bar{y}$ and Y increase with the frequency f under a constant duty cycle D, demonstrating a High-Pass FAC. (b) For a threshold of 0.359, G is positive at high duty cycles and negative at low duty cycles, indicating either a High-Pass FAC or a Low-Pass FAC. (c) With a threshold raised to 0.870, G becomes negative. Both $\bar{y}$ and Y decrease with the frequency f under a fixed duty cycle, showing a Low-Pass FAC. Moreover, the value of $\bar{y}$ is notably small.

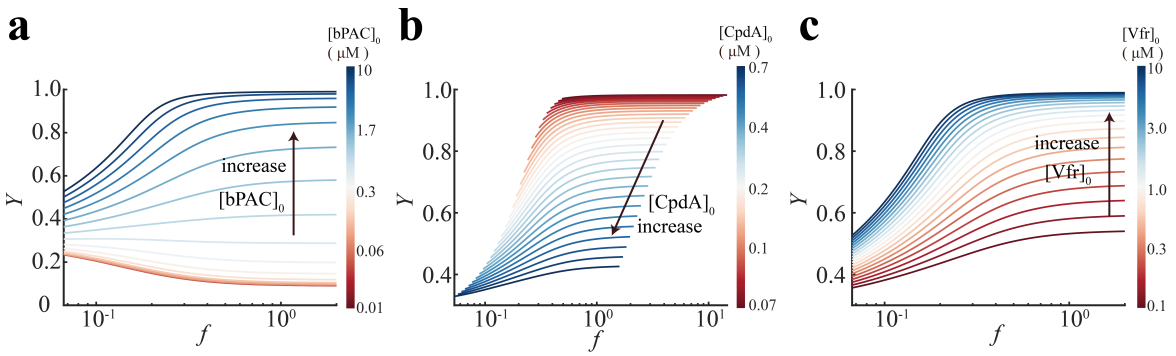

Supplementary Figure 3. Analytical solutions predict the impact of protein concentration on the performance of the FAC in the FDCC gene circuit. Explore the impact of protein expression levels of $[bPAC]_0$, $[CpdA]_0$,$[Vfr]_0$ in the genetic circuit on the FAC performance based on Formulas 6 and 10 in the main manuscript. (a) When λ equals 50 and γ equals 0.005, the output Y of the FAC system varies with frequency f as the bPAC concentration increases from 0.01 μM to 10 μM. (b) The curve of Y with frequency as the CpdA concentration varies, when λ is equal to 50. (c) When γ equals 0.005 and α equals 1, the curve of Y varies with frequency as the CpdA concentration changes.

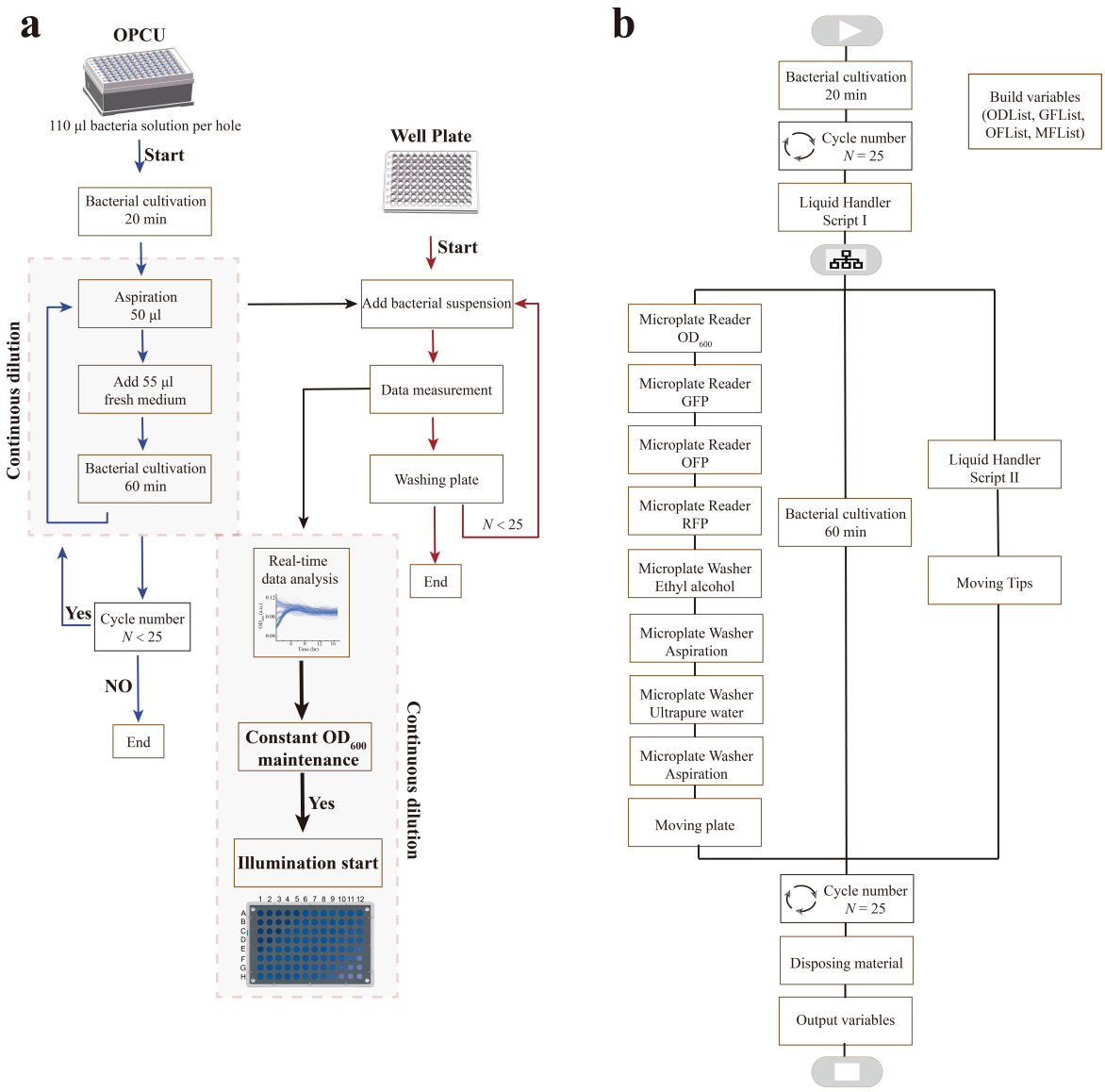

Supplementary Figure 4. Automated Experimental Workflow and Execution Script. (a) Schematic diagram of the continuous cultivation process in automated experiments. The blue lines represent the operation path of OPCU, while the red lines depict the operational path of the 96-well plate used for measurements. Bacterial suspension undergoes continuous dilution every hour to maintain a stable bacterial optical density OD_{600}, ensuring bacteria remain in the logarithmic growth phase for measurement accuracy. During the continuous dilution process, when the OD_{600} stabilizes at a constant value, initiate illumination. (b) The diagram illustrates the scripting of automated experiments controlling various devices on the automated island in software programming.

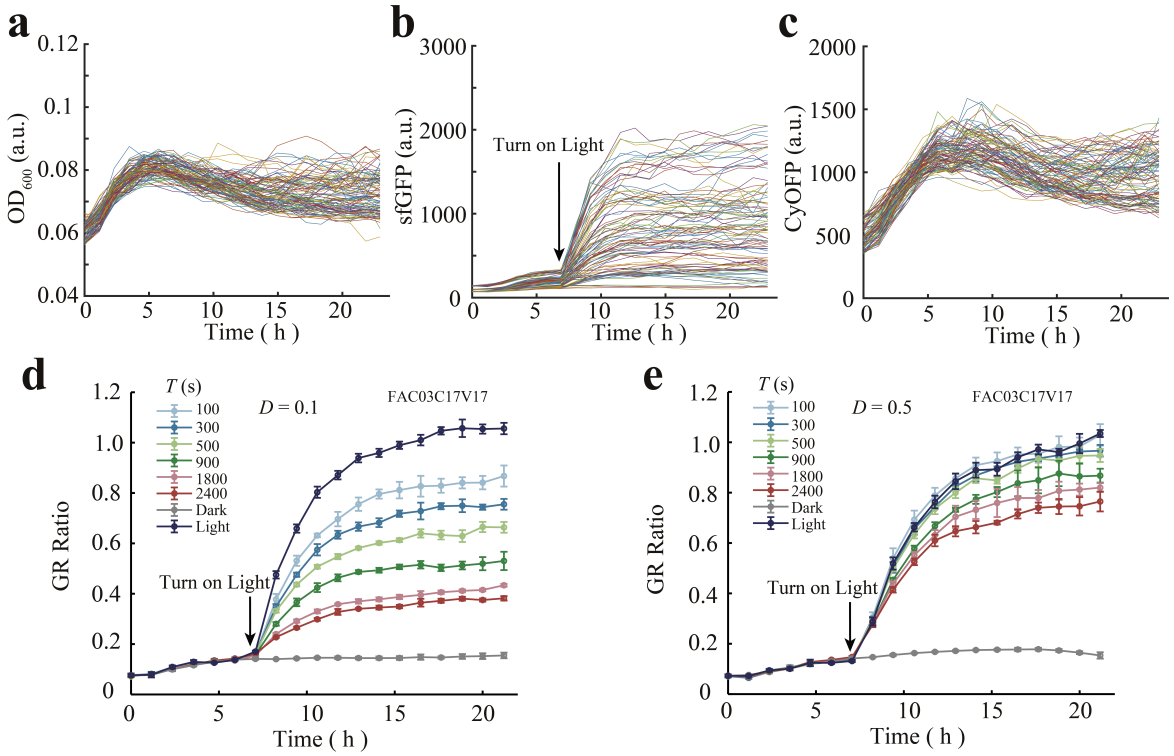

Supplementary Figure 5. Data Collection and Analysis in Automated Experiments. The raw values of absorbance OD_{600} (a), fluorescence GFP (b), and fluorescence CyOFP (c) intensities collected by the microplatereader in a single automated experiment with FAC03C17V17 strain (containing Plac-*sfGFP*-T0T1-J23102-*CyOFP*-pJN105) strain. Each well of the OPCU can be configured with varying light intensities I, periods P, and duty cycles D to characterize the FAC performance of the bacterial strain. Time-varying curve of the ratio of sfGFP fluorescence induced by the Plac promoter to the internal standard CyOFP fluorescence in the FAC03C17V17 strain when the duty cycle is 0.1 (d) and 0.5 (e) after cross-talk correction. Each curve represents a fixed period (100-300-500-900-1800-2400 seconds). The dark blue line represents the induction curve under continuous light exposure, while the gray line represents the induction curve without light exposure. The arrows in the diagram represent the timing for turning on the illumination. Once the ratios and OD values have stabilized, initiate the illumination with the OPCU. Each experiment was repeated three times, and error bars indicating standard deviation.

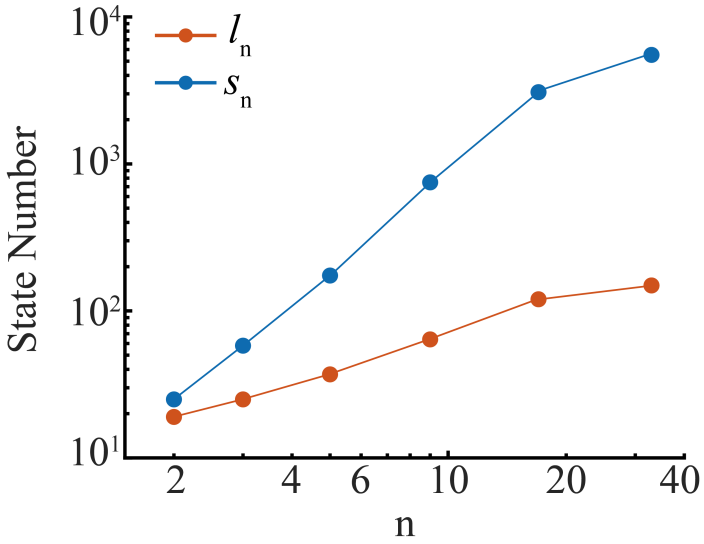

Supplementary Figure 6. Characterize the relationship between the number of states, information entropy and and the regulatory dimensionality using numerical analysis implemented in MATLAB. (a) Investigate the influence of regulatory dimensionality (specifically, the number of regulated proteins) on l_n and s_n. Here, l_n denotes the number of distinct grid cells crossed by the induction curve, generated by varying the duty cycle, in an n-dimensional expression space. This quantifies the discrete states attainable through duty cycle modulation. s_n represents the number of distinct grid cells covered by the n-dimensional parametric surface obtained by introducing Frequency Modulation. The lambda values for the regulatory proteins corresponding to the promoters are set as $(\lambda_1, \lambda_2, ..., \lambda_n) = (50, 50 \times 2^{2-1}, ..., 50 \times 2^{n-1})$. Discretization parameter $\epsilon = 0.1$. The blue curve illustrates the change of s_n with n, whereas the orange curve depicts the variation of l_n with n. The difference between s_n and l_n widens as n increases.

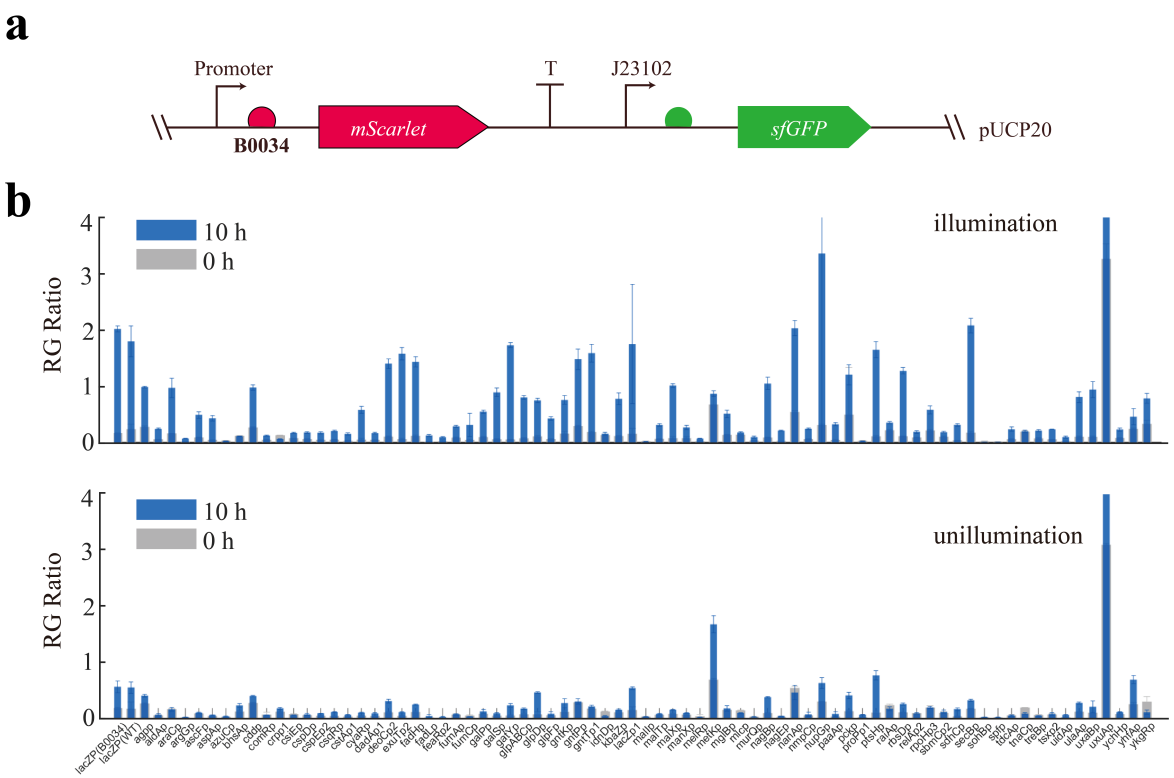

Supplementary Figure 7. High-throughput screening of cAMP-regulated promoters. (a) Plasmid schematic for screening cAMP-responsive promoters. The plasmids were transformed into the FAC03 strain, exposed to high-throughput blue light irradiation using the OPCU device, and fluorescent images of bacteria were captured under a microscope. (b) Quantitative analysis involves the ratio of induced mScarlet fluorescence intensity after 10 hours of illumination from the promoters to the sfGFP fluorescence intensity from the J23102 promoter. By comparing this ratio with the pre-illumination state (Top) and contrasting it with the data from a 10-hour culture without illumination (Bottom), significant cAMP-responsive promoters are identified. The sequences of the selected promoters are listed in Supplementary Table 8.

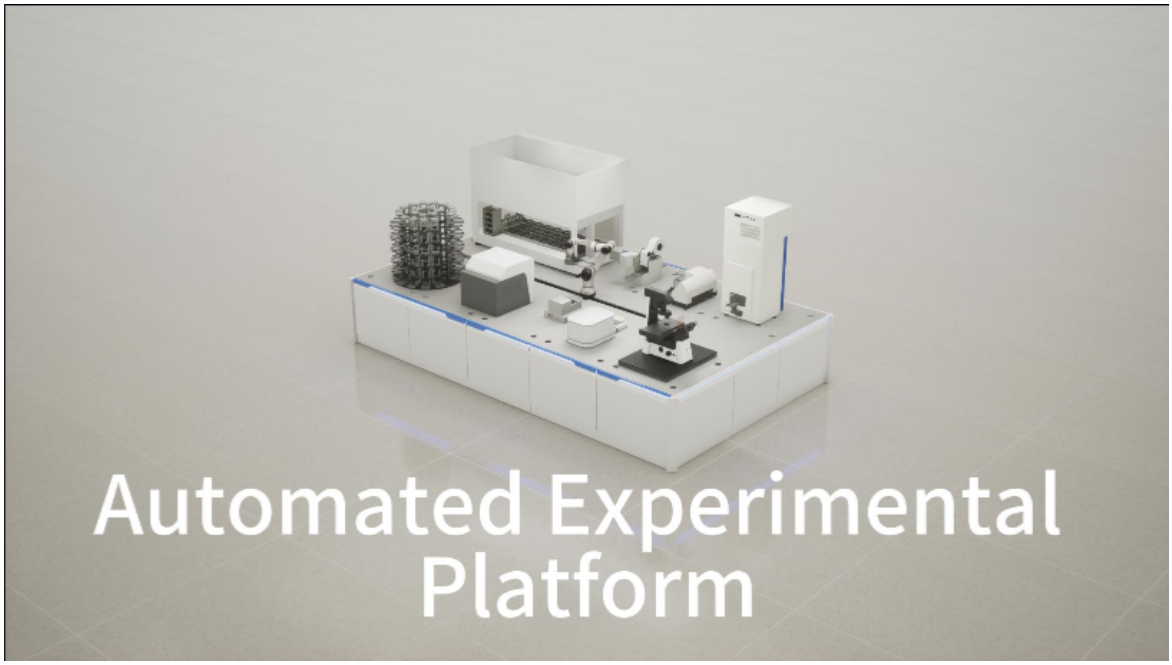

Supplementary Movie: Workflow of automated experiments. This video includes bacterial suspension dispensing, setting of illumination parameters, and the operation of automated island.

Section 3: Supplementary Tables

Supplementary Table.1: Chemical reactions in the CRN model.

		Reaction Equation	Description
M1	r1	$\text{bPAC}^* \xrightarrow{k_0} \text{bPAC}^* + \text{cAMP}$	Production of cAMP arising from the activated bPAC
	r2	$\text{cAMP} + \text{CpdA} \overset{k_r\ k_f}{\longleftrightarrow} \text{cAMP-CpdA}$	Degradation of cAMP arising from CpdA
M2	r3	$\text{cAMP-CpdA} \xrightarrow{\gamma} \text{CpdA}$	Degradation of cAMP arising from CpdA
	r4	$\text{cAMP} + \text{cAMP} + \text{Vfr} \overset{k_{\text{r1}}\ k_{\text{f1}}}{\longleftrightarrow} \text{Vfr-cAMP Complex}$	Formation of cAMP dependent transcription complex
	r5	$\text{Vfr-cAMP Complex} + \text{Plac} \overset{k_{\text{r2}}\ k_{\text{f2}}}{\longleftrightarrow} \text{Activated-Plac}$	Transcription initiation
M3	r6	$\text{Activated-Plac} \xrightarrow{k_1} \text{Activated-Plac} + \text{mRNA}$	Transcription of GFP
	r7	$\text{mRNA} \xrightarrow{k_{\text{deg1}}} \text{null}$	mRNA degradation
	r8	$\text{mRNA} \xrightarrow{k_2} \text{mRNA} + \text{GFP}$	Translation of GFP
	r9	$\text{GFP} \xrightarrow{k_{\text{deg2}}} \text{null}$	Protein degradation of GFP

Supplementary Table.2: Ordinary Differential Equations (ODEs) in the CRN model.

	Ordinary Differential Equations
Eq.1	$\frac{\mathrm{d}[\text{cAMP}]}{\mathrm{d}t} = k + k_{\mathrm{r}}[\text{cAMP-CpdA}] + k_{\mathrm{r1}}[\text{Vfr-cAMP Complex}] - k_{\mathrm{f}}[\text{cAMP}][\text{CpdA}] - k_{\mathrm{f1}}[\text{cAMP}][\text{Vfr}]^2$
Eq.2	$\frac{\mathrm{d}[\text{CpdA}]}{\mathrm{d}t} = (\alpha + k_{\mathrm{r}})[\text{cAMP-CpdA}] - k_{\mathrm{f}}[\text{cAMP}][\text{CpdA}]$
Eq.3	$\frac{\mathrm{d}[\text{cAMP-CpdA}]}{\mathrm{d}t} = k_{\mathrm{f}}[\text{cAMP}][\text{CpdA}] - (\alpha + k_r)[\text{cAMP-CpdA}]$
Eq.4	$\frac{\mathrm{d}[\text{Vfr}]}{\mathrm{d}t} = k_{\mathrm{r1}}[\text{Vfr-cAMP Complex}] - k_{\mathrm{f1}}[\text{Vfr}][\text{cAMP}]^2$
Eq.5	$\frac{\mathrm{d}[\text{Vfr-cAMP Complex}]}{\mathrm{d}t} = k_{\mathrm{f1}}[\text{Vfr}][\text{cAMP}]^2 - k_{\mathrm{r1}}[\text{Vfr-cAMP Complex}] + k_{\mathrm{r2}}[\text{Activated-Plac}] - k_{\mathrm{f2}}[\text{Vfr-cAMP Complex}][\text{Plac}]$
Eq.6	$\frac{\mathrm{d}[\text{Plac}]}{\mathrm{d}t} = k_{\mathrm{r2}}[\text{Activated-Plac}] - k_{\mathrm{f2}}[\text{Vfr-cAMP Complex}][\text{Plac}]$
Eq.7	$\frac{\mathrm{d}[\text{Activated-Plac}]}{\mathrm{d}t} = k_{\mathrm{f2}}[\text{Vfr-cAMP Complex}][\text{Plac}] - k_{\mathrm{r2}}[\text{Activated-Plac}]$
Eq.8	$\frac{\mathrm{d}[\text{mRNA}]}{\mathrm{d}t} = k_1[\text{Activated-Plac}] - k_{\mathrm{deg1}}[\text{mRNA}]$
Eq.9	$\frac{\mathrm{d}[\text{GFP}]}{\mathrm{d}t} = k_2[\text{mRNA}] - k_{\mathrm{deg2}}[\text{GFP}]$

Supplementary Table.3: Kinetetic parameters in the CRN model.

Kinetic Constant	Description	Value	Unit	Notes
k_0	rate of cAMP production from bPAC*	0.0045	s^{-1}	
k	rate of cAMP production from bPAC*, which includes the influence of bPAC* concentration	0.0045	$\mu M \cdot s^{-1}$	$k = k_0[\text{bPAC}^*]$
k_f	binding constant of cAMP and CpdA	10	$(\mu M \cdot s)^{-1}$	
k_r	dissociation constant of cAMP and CpdA	70	s^{-1}	
γ	rate of degradation of cAMP-CpdA	0.069	s^{-1}	
k_{f1}	binding constant of Vfr and cAMP	20	$(\mu M^2 \cdot s)^{-1}$	
k_{r1}	dissociation constant of Vfr and cAMP	80	s^{-1}	$K_1 = \sqrt{\frac{k_{r1}}{k_{f1}}}$
k_{f2}	binding constant of Vfr-cAMP$_2$ Complex and Plac	100	$(\mu M \cdot s)^{-1}$	
k_{r2}	dissociation constant of Vfr-cAMP$_2$ Complex and Plac	1	s^{-1}	$K_2 = \frac{k_{r2}}{k_{f2}}$
k_1	rate of transcription of GFP from Activated-Plac	6×10^{-4}	s^{-1}	
k_2	rate of translation of GFP from mRNA	3.5×10^{-3}	s^{-1}	
k_{deg1}	rate of mRNA degradation	5×10^{-3}	s^{-1}	
k_{deg2}	rate of GFP degradation	2.7×10^{-4}	s^{-1}	

Supplementary Table.4: The symbols and their meanings used in this study.

Symbols	Unit	Physical Significance
k	$\mu M \cdot s^{-1}$	Synthetic rate of cAMP mediated by bPAC*
γ	s^{-1}	hydrolysis rate of cAMP mediated by CpdA
x	μM	concentration of cAMP
$x_1,\ x_2$	μM	concentration of cAMP during the light and dark periods, respectively
$x_H,\ x_L$	μM	initial concentration of cAMP at the beginning of the light or dark period
t	s	time
T	s	period of square-wave signal
I	$\mu W \cdot cm^{-2}$	light intensity
K_1	μM	The microscopic dissociation constant between cAMP and the transcription factor Vfr represents the affinity of the interaction, with the concentration of cAMP being the ligand concentration required to achieve half-maximal binding of Vfr.
K_2	μM	The microscopic dissociation constant for the Vfr-$cAMP_2$ Complex binding to regulatory promoters reflects the affinity of the complex for these promoters, with the concentration of the Vfr-$cAMP_2$ Complex being the ligand concentration required to achieve half-maximal binding of the promoters.
D	non-dimensional	Duty cycle (D) is the fraction of one period in which the light is active, defined as $D = \frac{PW}{T}$, where PW is the active time of the light.
τ	non-dimensional	Non-dimensional time, defined as $\tau = t\gamma$.
ϕ	non-dimensional	Non-dimensional representation of the light period, defined as $\phi = T\gamma$.
f	non-dimensional	Non-dimensional frequency of the period, calculated as $f = \frac{1}{\phi} = \frac{1}{\gamma T}$.

Continued on next page

Symbols	Unit	Physical Significance
$s(s_1, s_2)$	non-dimensional	The non-dimensional representation of cAMP concentration is defined as $s = x/\frac{k}{\gamma}$,where $\frac{k}{\gamma}$ represents the theoretical maximum concentration of cAMP.
$s_{\mathrm{H}}, s_{\mathrm{L}}$	non-dimensional	Highest and lowest non-dimensional concentrations of cAMP in one period.
α	non-dimensional	Parameter representing light intensity, defined as $\alpha = \frac{k}{\gamma K_1}$.
λ	non-dimensional	Non-dimensional parameter representing the relative abundance of transcription factor Vfr, defined as $\lambda = \frac{[\mathrm{Vfr}]_0}{K_2}$.
θ	non-dimensional	Defined parameter for equation simplification, defined as $\theta = \lambda\alpha^2$.
ψ	non-dimensional	Fraction of activated promoters, calculated as: $\psi = \frac{1}{1+\frac{1}{\lambda}(1+\frac{1}{\alpha^2 s^2})}$
$\bar{y}$	non-dimensional	Steady-state average non-dimensional GFP concentration over one period, defined as: $\bar{y} = f\int_0^{1/f}\psi(\tau)\mathrm{d}\tau$
y^*	non-dimensional	Steady-state average GFP concentration over one constant light period, defined as: $y^* = \bar{y}(D=1)$
s^*	non-dimensional	Threshold of M2 filter, representing the non-dimensional concentration of cAMP, is defined as: $s^* = s(\psi''=0)$
Y	non-dimensional	Non-dimensional representation of protein concentration, defined as: $Y = \frac{\bar{y}}{y^*}$
$Y_{\mathrm{HF}}, Y_{\mathrm{LF}}$	non-dimensional	The non-dimensional representation of protein concentration, as the non-dimensionalized frequency f approaches its theoretical limits, is defined $Y_{\mathrm{HF}} = \lim_{f\to\infty} Y$ by for high-frequency conditions and $Y_{\mathrm{LF}} = \lim_{f\to 0} Y$ for low-frequency condition. At experimental conditions, frequency is usually between 1/100 s^{-1} and 1/2400 s^{-1}, which is constrained by the period of strain division cycle.

Continued on next page

Symbols	Unit	Physical Significance
G	non-dimensional	Non-dimensional representation of frequency influence on the protein output, defined as: $G = f\left[\ln\left(\sqrt{\frac{1+(\frac{s_{\mathrm{H}}}{\sqrt{3}s^*})^2}{1+(\frac{s_{\mathrm{L}}}{\sqrt{3}s^*})^2}}\right) - \sqrt{3}s^*\left(\tan^{-1}\frac{\frac{s_{\mathrm{H}}}{\sqrt{3}s^*}-\frac{s_{\mathrm{L}}}{\sqrt{3}s^*}}{1+\frac{s_{\mathrm{H}}}{\sqrt{3}s^*}\frac{s_{\mathrm{L}}}{\sqrt{3}s^*}}\right)\right]$

Supplementary Table.5: The effect of experimental control parameters on the characteristics of FAC.

Tunable Parameters		Description	Corresponding Parameters	
Signal input parameters	I	Light intensity	α	$\alpha = \frac{k}{\gamma K_1}$
	T	Period of square-wave signal	f	$f = \frac{1}{\phi} = \frac{1}{\gamma T}$
	D	Duty cycle of square-wave signal	$D, s_{\mathrm{H}}, s_{\mathrm{L}}$	$s_{\mathrm{H}} = \frac{1-e^{-\phi D}}{1-e^{-\phi}}$
				$s_{\mathrm{L}} = \frac{e^{\phi D}-1}{e^{\phi}-1}$
System parameters in gene circuit	$[\mathrm{bPAC}]_0$	the initial concentration of bPAC protein	α	
	$[\mathrm{CpdA}]_0$	the initial concentration of CpdA protein	$s_{\mathrm{H}}, s_{\mathrm{L}}, f, \alpha$	
	$[\mathrm{Vfr}]_0$	the initial concentration of Vfr protein	$\lambda, f, s_{\mathrm{H}}, s_{\mathrm{L}}$	$\lambda = \frac{[\mathrm{Vfr}]_0}{K_2}$

Supplementary Table.6: Bacterial strains used in this study.

P.aeruginosa strains	Description	Source
FAC01	Knockout six gens (*exoS, exoT, pslBCD, pelA, cyaA and cyaB*) in wild-type strain PAO1.	This study
FAC03	FAC01, Genomic insertion of *bPAC* fragment using plasmid PA1/O4/O3-*bPAC*-CTX2.	This study
FAC03C04V04	FAC03, the promoters and RBS of *vfr* and *cpdA* on the genome have been replaced with J23102-RBS004 and J23100-RBS004, respectively. Containing plasmid Plac-*sfGFP*-T0T1-J23102-*CyOFP*-pJN105.	This study
FAC03C04V17	FAC03, the promoters and RBS of *vfr* and *cpdA* on the genome have been replaced with J23102-RBS017 and J23100-RBS004, respectively. Containing plasmid Plac-*sfGFP*-T0T1-J23102-*CyOFP*-pJN105.	This study
FAC03C17V34	FAC03, the promoters and RBS of *vfr* and *cpdA* on the genome have been replaced with J23102-B0034 and J23100-RBS017, respectively. Containing plasmid Plac-*sfGFP*-T0T1-J23102-*CyOFP*-pJN105.	This study
FAC03C17V46	FAC03, the promoters and RBS of *vfr* and *cpdA* on the genome have been replaced with J23102-RBS046 and J23100-RBS017, respectively. Containing plasmid Plac-*sfGFP*-T0T1-J23102-*CyOFP*-pJN105.	This study
FAC03C17V17	FAC03, the promoters and RBS of *vfr* and *cpdA* on the genome have been replaced with J23102-RBS017 and J23100-RBS017, respectively. Containing plasmid Plac-*sfGFP*-T0T1-J23102-*CyOFP*-pJN105.	This study
FAC03C21V34	FAC03, the promoters and RBS of *vfr* and *cpdA* on the genome have been replaced with J23102-B0034 and J23100-RBS021, respectively. Containing plasmid Plac-*sfGFP*-T0T1-J23102-*CyOFP*-pJN105.	This study

Continued on next page

P.aeruginosa strains	Description	Source
FAC01C17V34B17	FAC01, the promoters and RBS of *vfr* and *cpdA* on the genome have been replaced with J23102-B0034 and J23100-RBS017, respectively. Genomic insertion of bPAC fragment using plasmid PA1-RBS017-bPAC-CTX2. Containing plasmid Plac-*sfGFP*-T0T1-J23102-*CyOFP*-pJN105.	This study
FAC03C02V34	FAC03, the promoters and RBS of *vfr* and *cpdA* on the genome have been replaced with J23102-B0034 and J23100-RBS002, respectively. Containing plasmid Plac-*sfGFP*-T0T1-J23102-*CyOFP*-pJN105.	This study
FAC03C10V34	FAC03, the promoters and RBS of *vfr* and *cpdA* on the genome have been replaced with J23102-B0034 and J23100-RBS010, respectively. Containing plasmid Plac-*sfGFP*-T0T1-J23102-*CyOFP*-pJN105.	This study
FAC03C14V34	FAC03, the promoters and RBS of *vfr* and *cpdA* on the genome have been replaced with J23102-B0034 and J23100-RBS014, respectively. Containing plasmid Plac-*sfGFP*-T0T1-J23102-*CyOFP*-pJN105.	This study
FAC03C16V34	FAC03, the promoters and RBS of *vfr* and *cpdA* on the genome have been replaced with J23102-B0034 and J23100-RBS016, respectively. Containing plasmid Plac-*sfGFP*-T0T1-J23102-*CyOFP*-pJN105.	This study
FAC03C20V34	FAC03, the promoters and RBS of *vfr* and *cpdA* on the genome have been replaced with J23102-B0034 and J23100-RBS020, respectively. Containing plasmid Plac-*sfGFP*-T0T1-J23102-*CyOFP*-pJN105.	This study
FAC03C22V34	FAC03, the promoters and RBS of *vfr* and *cpdA* on the genome have been replaced with J23102-B0034 and J23100-RBS022, respectively. Containing plasmid Plac-*sfGFP*-T0T1-J23102-*CyOFP*-pJN105.	This study

Continued on next page

P.aeruginosa strains	Description	Source
FAC03C02V17	FAC03, the promoters and RBS of *vfr* and *cpdA* on the genome have been replaced with J23102-RBS017 and J23100-RBS002, respectively. Containing plasmid Plac-*sfGFP*-T0T1-J23102-*CyOFP*-pJN105.	This study
FAC03C10V17	FAC03, the promoters and RBS of *vfr* and *cpdA* on the genome have been replaced with J23102-RBS017 and J23100-RBS010, respectively. Containing plasmid Plac-*sfGFP*-T0T1-J23102-*CyOFP*-pJN105.	This study
FAC03C14V17	FAC03, the promoters and RBS of *vfr* and *cpdA* on the genome have been replaced with J23102-RBS017 and J23100-RBS014, respectively. Containing plasmid Plac-*sfGFP*-T0T1-J23102-*CyOFP*-pJN105.	This study
FAC03C16V17	FAC03, the promoters and RBS of *vfr* and *cpdA* on the genome have been replaced with J23102-RBS017 and J23100-RBS016, respectively. Containing plasmid Plac-*sfGFP*-T0T1-J23102-*CyOFP*-pJN105.	This study
FAC03C20V17	FAC03, the promoters and RBS of *vfr* and *cpdA* on the genome have been replaced with J23102-RBS017 and J23100-RBS020, respectively. Containing plasmid Plac-*sfGFP*-T0T1-J23102-*CyOFP*-pJN105.	This study
FAC03C22V17	FAC03, the promoters and RBS of *vfr* and *cpdA* on the genome have been replaced with J23102-RBS017 and J23100-RBS022, respectively. Containing plasmid Plac-*sfGFP*-T0T1-J23102-*CyOFP*-pJN105.	This study
FAC03C10V04	FAC03, the promoters and RBS of *vfr* and *cpdA* on the genome have been replaced with J23102-RBS004 and J23100-RBS010, respectively. Containing plasmid Plac-*sfGFP*-T0T1-J23102-*CyOFP*-pJN105.	This study

Continued on next page

P.aeruginosa strains	Description	Source
FAC03C20V04	FAC03, the promoters and RBS of *vfr* and *cpdA* on the genome have been replaced with J23102-RBS004 and J23100-RBS020, respectively. Containing plasmid Plac-*sfGFP*-T0T1-J23102-*CyOFP*-pJN105.	This study
FAC03C23115V04	FAC03, the promoters and RBS of *vfr* and *cpdA* on the genome have been replaced with J23102-RBS004 and J23115-B0034, respectively. Containing plasmid Plac-*sfGFP*-T0T1-J23102-*CyOFP*-pJN105.	This study
FAC03C02V04	FAC03, the promoters and RBS of *vfr* and *cpdA* on the genome have been replaced with J23102-RBS004 and J23100-RBS002, respectively. Containing plasmid Plac-*sfGFP*-T0T1-J23102-*CyOFP*-pJN105.	This study
FAC03C14V04	FAC03, the promoters and RBS of *vfr* and *cpdA* on the genome have been replaced with J23102-RBS004 and J23100-RBS014, respectively. Containing plasmid Plac-*sfGFP*-T0T1-J23102-*CyOFP*-pJN105.	This study
FAC03C22V04	FAC03, the promoters and RBS of *vfr* and *cpdA* on the genome have been replaced with J23102-RBS004 and J23100-RBS022, respectively. Containing plasmid Plac-*sfGFP*-T0T1-J23102-*CyOFP*-pJN105.	This study
FAC03C23106V04	FAC03, the promoters and RBS of *vfr* and *cpdA* on the genome have been replaced with J23102-RBS004 and J23106-B0034, respectively. Containing plasmid Plac-*sfGFP*-T0T1-J23102-*CyOFP*-pJN105.	This study
FAC03C23106V34	FAC03, the promoters and RBS of *vfr* and *cpdA* on the genome have been replaced with J23102-B0034 and J23106-B0034, respectively. Containing plasmid Plac-*sfGFP*-T0T1-J23102-*CyOFP*-pJN105.	This study

Continued on next page

P.aeruginosa strains	Description	Source
FAC03C23115V34	FAC03, the promoters and RBS of *vfr* and *cpdA* on the genome have been replaced with J23102-B0034 and J23115-B0034, respectively. Containing plasmid Plac-*sfGFP*-T0T1-J23102-*CyOFP*-pJN105.	This study
FAC03C23106V17	FAC03, the promoters and RBS of *vfr* and *cpdA* on the genome have been replaced with J23102-RBS017 and J23106-B0034, respectively. Containing plasmid Plac-*sfGFP*-T0T1-J23102-*CyOFP*-pJN105.	This study.
FAC03C23115V17	FAC03, the promoters and RBS of *vfr* and *cpdA* on the genome have been replaced with J23102-RBS017 and J23115-B0034, respectively. Containing plasmid Plac-*sfGFP*-T0T1-J23102-*CyOFP*-pJN105.	This study.
FAC03C17V17-NP	FAC03, the promoters and RBS of *vfr* and *cpdA* on the genome have been replaced with J23102-RBS017 and J23100-RBS017, respectively. Without plasmid Plac-*sfGFP*-T0T1-J23102-*CyOFP*-pJN105.	This study.
AutoRGB	FAC03C17V17-NP, Genomic insertion of nupGp-sfGFP fragments using plasmid PA3781-nupGp-*sfGFP*-noBBA-PCRISPR.	This study.
AutoRGB-6	AutoRGB, containing plasmid nanAp-*mScarlet*-Plac-*CyOFP*-pJN105.	This study.
AutoRGB-9	AutoRGB, containing plasmid nanAp-*mScarlet*-J23102-*CyOFP*-pJN105.	This study.

492 **Supplementary Table.7: Plasmids used in this study.**

Plasmid	Description	Source
PCASPA	Plasmid expression Cas9 for chromosomal insertion of deletion. Tet^r	ref 1
PCRISPR	Plasmid expression gRNA for chromosomal insertion of deletion. Carb^r	ref 1
PA3781-nupGp-*sfGFP*-noBBA-PCRISPR	Plasmid used for inserting nupGp-sfGFP fragment into the genome.	This study.
PCRISPR-*cyaA*	Plasmid used knock out *cyaA*. Carb^r	This study.
PCRISPR-*cyaB*	Plasmid used knock out *cyaA*. Carb^r	This study.
PCRISPR-*exoS*	Plasmid used knock out textitexoS. Carb^r	This study.
PCRISPR-*exoT*	Plasmid used knock out *exoT*. Carb^r	This study.
PCRISPR-*pslBCD*	Plasmid used knock out *pslBCD*. Carb^r	This study.
PCRISPR-*pelA*	Plasmid used knock out pelA. Carb^r	This study.
J23102-B0034-*vfr*-PCRISPR	Plasmid used for replacing the promoter of *vfr* with J23102-B0034. Carb^r	This study.
J23102-RBS046-*vfr*-PCRISPR	Plasmid used for replacing the promoter of *vfr* with J23102-RBS046. Carb^r	This study.
J23102-RBS004-*vfr*-PCRISPR	Plasmid used for replacing the promoter of *vfr* with J23102-RBS004. Carb^r	This study.
J23102-RBS017-*vfr*-PCRISPR	Plasmid used for replacing the promoter of *vfr* with J23102-RBS017. Carb^r	This study.
J23102-B0034-*cpdA*-PCRISPR	Plasmid used for replacing the promoter of *cpdA* with J23102-B0034. Carb^r	This study.
J23102-RBS046-*cpdA*-PCRISPR	Plasmid used for replacing the promoter of *cpdA* with J23102-RBS046. Carb^r	This study.
J23102-RBS004-*cpdA*-PCRISPR	Plasmid used for replacing the promoter of *cpdA* with J23102-RBS004. Carb^r	This study.
J23102-RBS017-*cpdA*-PCRISPR	Plasmid used for replacing the promoter of *cpdA* with J23102-RBS017. Carb^r	This study.

Ref 1. doi: 10.1016/j.isci.2018.07.024

Continued on next page

Plasmid	Description	Source
J23102-RBS021-*cpdA*-PCRISPR	Plasmid used for replacing the promoter of *cpdA* with J23102-RBS021. Carb^r	This study.
PA1-RBS017-*bPAC*-CTX2	Plasmid used for chromosomal insertion of PA1-RBS017-*bPAC* at attB site. Tetr	This study.
PA1O4O3-*bPAC*-CTX2	Plasmid used for chromosomal insertion of PA1O4O3-*bPAC* at attB site. Tetr	This study.
J23102-RBS002-*cpdA*-PCRISPR	Plasmid used for replacing the promoter of *cpdA* with J23102-RBS002. Carb^r	This study.
J23102-RBS010-*cpdA*-PCRISPR	Plasmid used for replacing the promoter of *cpdA* with J23102-RBS010. Carb^r	This study.
J23102-RBS014-*cpdA*-PCRISPR	Plasmid used for replacing the promoter of *cpdA* with J23102-RBS014. Carb^r	This study.
J23102-RBS016-*cpdA*-PCRISPR	Plasmid used for replacing the promoter of *cpdA* with J23102-RBS016. Carb^r	This study.
J23102-RBS020-*cpdA*-PCRISPR	Plasmid used for replacing the promoter of *cpdA* with J23102-RBS020. Carb^r	This study.
J23102-RBS022-*cpdA*-PCRISPR	Plasmid used for replacing the promoter of *cpdA* with J23102-RBS022. Carb^r	This study.
J23106-B0034-*cpdA*-PCRISPR	Plasmid used for replacing the promoter of *cpdA* with J23106-B0034. Carb^r	This study.
J23115-B0034-*cpdA*-PCRISPR	Plasmid used for replacing the promoter of *cpdA* with J23115-B0034.	This study.
J23110-B0034-*cpdA*-PCRISPR	Plasmid used for replacing the promoter of *cpdA* with J23110-B0034. Carb^r	This study.
Plac-*sfGFP*-T0T1-J23102-*CyOFP*-pJN105	cAMP reporter plasmid. Gm^r	This study.
nanAp-*mScarlet*-J23102-*CyOFP*-pJN105	Expression reporter protein mScarletI under control of nanAp ptomoter. Gm^r	This study.
nanAp-*mScarlet*-Plac-*CyOFP*-pJN105	Expression reporter protein mScarletI and CyOFP under control of nanAp and Plac ptomoter, respectively. Gm^r	This study.

Supplementary Table.8: Sequence list of screened cAMP responsive promoters.

Promoter	Sequence
nanAp	TCTCTGCTACCTGGCACGCTTTCGGTCAGACCACCAACAAAAAGAAATAATG CCACTTTAGTGAAGCAGATCGCATTATAAGCTTTCTGTATGGGGTGTTGCTT AATTGATCTGGTATAACAGGTATAAAGGTATATCGTTTATCAGACAAGCATC ACTTCAGAGGTATTT
galSp	CGATCTGGATCACATTCGTTAACAAAACGGCTGTAACCGTTTCCATTGCTGT GACTCGATTCACGAAGTCCTGTATTCAGTGCTGACAAAATAGCCGCCAG CAAGCAGTCATTTACTGCAATCTCATAACAGGTAGTGAAT
pcKp	GTTGAATTTGCATCAATTTCATTCAGGAATGCGATTCCACTCACAATATTCCC GCCATATAAACCAAGATTTAACCTTTTGAGAACATTTTCCACACCTAAAATG CTATTTCTGCGATAATAGCAACCGTTTCGTGACAGGAATCACGGAGTTTTTT GTCAAATATGAATTTCTCCAGATACGTAAATCTATGAGCCTTGTCGCGGTTA ACACCCCCAAAAAGACTTTACTATTCAGGCAATACATATTGGCTAAGGAGCA GTGAA
exuTp2	CGAAGATATTTTCGTGAGTTAGATCAATAAACGTAGTTAAAAAAATTACTC TCAAAGTGGTAAATCTCGCTGCAGGCCGCGCCAGTACTGGCCTTGCTGTCG TCAGGTAATGTCCCTACAAATATTCCCACATTTGTGATGGCTCTCACCTT TTAAAGTTGTATGACAAGTTATCTTTCTGCCGTCGCAAATCATAAGTCGA CGGAATGCAAATTGCCGATTCATTCATTTGTTAGATGAATCGGGTTAACC GGTACGGAAGCCGAATTAGCACGAAACTTTCATGGCAACGTTCGGGGCGT GCCGGTTTTTTTTCGGTTACCCGGTCGTAACTAACATCTTCAGCCTCTGG CGGGATGATGGCCGCGCTTCCTGCGGATATAACAAAACGATGAGGTTTTAC
nupGp	CGCCCCTGACGATGCTCAGGGGCAAAAATGTTATCCACATCACAATTTCGTT TTGCAAATTGGGAATGTTTGCAATTATTTGCCACAGGTAACAAAAAACCA GTCCGCGAAGTTGATAGAATCCCATCATCTCGCACGGTCAAATGTGCTTT TTCAAACACTCATCCGCATCACGATGTGAGGAAATTAACATG
deoCp2	GAAAGTGAATTATTTGAACCAGATCGCATTACAGTGATGCAAACTTGTAAG TAGATTTCCTTAATTGTGATGTGTATCGAAGTGTGTTGCGGAGTAGATGT TAGAATACTAACAAACTCGCAAGGTGAATTTTATTGGCGACAAGCCAGGA GAATGAA
gatYp	ACTTTGCTACGGCTTCCCTATCGGGAGGCCGTTTTTTTGCCTTTCACTCCT CGAATAATTTTCATATTGTCGTTTTTGTGATCGTTATCTCGATATTTAAA AACAAATAATTTCATTATATTTTGAAATCGAAAACAAACGACAGGATATG AAA
paaAp	GCGGAAAACATTAATGCACTGATAAATAATGATTTATAAAAATAGGGTGCG AAATCCGTCACAGTTCAAACATACAAAATTTGTGATTTTACTTAACTATT GTGTAACTTTCATAAAACAATGTGATTCGTGTTTTTAATTAATTCACGAA AACTGGAATCGTAAAGGTGATGAC
glpABCp	CATTCATAAATTAAATGTGAATTGCCGCACACATTATTAAATAAGATTT ACAAAATGTTCAAAATGACGCATGAAATCACGTTTCACTTTCGAATTATG AGCGAATATGCGCGAAATCAAACAATTCATGTTTTTACTATGGCTAAATG GTAAAAAACGAACTTCAGAGGGATAACA